

Laser pulse-length effects in trident pair production

U. Hernandez Acosta and B. Kämpfer

Helmholtz-Zentrum Dresden-Rossendorf, POB 51 01 19, 01314 Dresden, Germany
TU Dresden, Institut für Theoretische Physik, 01062 Dresden, Germany

E-mail: u.hernandez@hzdr.de

5 June 2019

Abstract. Laser pulses facilitate multiphoton contributions to the trident pair production $e_L^- \rightarrow e_L^- + e_L^+ + e_L^-$, where the label L indicates a laser field dressed electron (e^-) or positron (e^+). We isolate the impact of the pulse envelope in the trident S matrix element, formulated within the Furry picture, in leading order of a series expansion in the classical non-linearity parameter a_0 . Generally, the Fourier transform of the envelope carries the information on the pulse length, which becomes an easily tractable function in the case of a \cos^2 pulse envelope. The transition to a monochromatic laser wave can be handled in a transparent manner, as also the onset of bandwidth effects for short pulses can be factorized out and studied separately.

1 Introduction

High-intensity laser beams in the optical regime are customarily generated by the chirped pulse amplification (cf. [1]). Intensities up to $10^{22} \frac{\text{W}}{\text{cm}^2}$ are achievable nowadays in several laboratories [2], yielding a classical non-linearity parameter of $a_0 = \mathcal{O}(10 - 50)$ in the focal spot[‡]. Ongoing projects [4, 5, 6] of 10 PW class lasers envisage even larger values of a_0 . Due to higher frequencies in XFEL beams, $\omega = \mathcal{O}(10 \text{ keV})$, the parameter a_0 stays significantly below unity, despite similar intensities of $\mathcal{O}(10^{22} \frac{\text{W}}{\text{cm}^2})$ when tight focusing is attained [7]. Given such a variety of laser facilities, the experimental exploration of nonlinear QED effects became feasible and is currently further promoted. Elementary processes are under consideration with the goal of testing QED in the strong-field regime. Most notable is the nonlinear Compton process $e_L^- \rightarrow e_L^- + \gamma$, also w.r.t. the subsequent use of the high energy photons (γ), up to prospects of industrial applications. While in the pioneering theoretical studies [8, 9] the higher harmonics, related to multi-photon effects, i.e. the simultaneous interaction of the electron with a multitude of photons, in monochromatic laser beams have been considered, the study of laser pulses revealed a multitude of novel structures in the γ spectrum [3, 10, 11, 12, 13, 14, 15, 16, 17, 18].

The nonlinear Breit-Wheeler process, $\gamma \rightarrow e_L^- + e_L^+$ [19, 20, 3, 21, 13, 22, 23, 24, 25, 26, 27, 28, 29], as cross channel of the nonlinear Compton process, is in contrast a threshold process – sometimes termed a genuine quantum process – since the probe photon γ energy in combination with the laser must supply sufficient energy to produce a e^+e^- pair. When considering the seminal SLAC experiment E-144 [30, 31] as a two-step process (first step: generation of a high-energy photon γ by Compton backscattering [32], second step: Breit-Wheeler process $\gamma + L \rightarrow e^+e^-$), also the nonlinear Breit-Wheeler process has been identified with the simultaneous interaction of up to five photons in the elementary subprocess.

Strictly speaking, the mentioned two-step process is only a part of trident pair production $e_L^- \rightarrow e_L^- + e_L^+ + e_L^-$, as stressed in [33, 34]. Since the trident process is the starting point of seeded QED avalanches, expected to set in at high-intensities, it is currently a subject of throughout analyses [35, 36, 37], also for benchmarking PIC codes [38].

Given the high repetition rate of the European XFEL [39] a potentially interesting option is to combine it with a synchronized electron beam of about 50 MeV (to operate slightly above the threshold) in order to facilitate a high-statistics search for the dark photon. Such a dark photon (also dubbed U boson or hidden photon) is a candidate for Dark Matter beyond the standard model of particle physics; it is a possible extension which enjoys intense theoretical [40, 41, 42] and experimental [43, 44, 45, 46] considerations. A corresponding theoretical analysis of the trident process can be found in [47]. In fact, the trident process – in a perturbative QED language – includes sub-diagrams of the type $\gamma^* \rightarrow e^+e^-$, i.e. an intermediate (virtual) photon which decays into a e^+e^- pair.

[‡] The relation of a_0 vs. the laser peak intensity I_L and frequency ω reads $a_0 \simeq 7.5 \frac{\text{eV}}{\omega} \sqrt{\frac{I_L}{10^{20} \text{ W/cm}^2}}$, cf. [3].

Via kinetic mixing, that virtual photon may “temporarily” couple to a dark photon A' , e.g. $\gamma^* \rightarrow A' \rightarrow \gamma^*$, thus signaling its presence as a peak of the invariant mass distribution of e^+e^- . The peak would be at the mass of the dark photon and its width is related to the kinetic mixing strength.

We briefly mention the trident option of the LUXE project [48, 49] at DESY/Hamburg, which however is primarily dedicated to explore the “boiling of the vacuum” by means of the nonlinear Breit-Wheeler process in the Ritus corner, i.e. a kinematical region with a nonperturbative field strength dependence and coupling constant $|e|$ dependence analog to the Schwinger pair creation probability.

While most of the above quoted papers focus on nonlinear effects in strong laser pulses, that is the impact of multiphoton contributions, we aim here at the study of apparent multiphoton effects due to bandwidth effects in weak and moderately strong laser pulses with $a_0 < 1$. The analysis of the Breit-Wheeler pair production in [22, 50] revealed that in such a regime interesting features appear for short and ultra-short pulses. For instance, despite of $a_0 < 1$ a significant subthreshold pair production is enabled. Roughly speaking, in short pulses the frequency spectrum contains high Fourier components, thus enabling the subthreshold pair creation. In that respect, we are going to study the relevance of the pulse duration for the trident process. In contrast to the elementary one-vertex processes, the trident process as a two-vertex process obeys a higher complexity, similar to the two-photon Compton scattering [51, 52, 53].

Our paper is organised as follows. In section 2, the matrix element is evaluated with emphasis on a certain regularisation required to uncover the perturbative limit. The weak-field expansion is presented in section 3, where the Fourier transform of the background field amplitude is highlighted as a central quantity. The case of a \cos^2 envelope is elaborated in some detail in section 4, where also numerical examples are exhibited. The conclusion can be found in section 5.

2 Matrix element in the Furry picture

The leading-order tree level Feynman diagram of the trident process is exhibited in figure 1(a). The corresponding S matrix reads

$$S_{fi} = e^2 \int d^4x \int d^4y \left[\left(\bar{\psi}(x; p_1) \gamma^\mu \psi(x; p) \right) D_{\mu\nu}(x - y) \left(\bar{\psi}(y; p_2) \gamma^\nu \psi^{(+)}(y; p_3) \right) - (p_1 \leftrightarrow p_2) \right], \quad (1)$$

where $\psi(x; p)$ stands for the Volkov solution of Dirac’s equation with a classical external electromagnetic (laser) field $A_\mu(\phi) = a_0 \frac{m}{|e|} \varepsilon_\mu f(\phi)$, $\bar{\psi}$ its adjoint, and $D_{\mu\nu}$ is the photon propagator. The $p_1 \leftrightarrow p_2$ term ensures the antisymmetrization of two identical fermions (mass m , charge $|e|$) in the final state. The laser field A_μ and its polarisation four-vector ε_μ and phase $\phi = k \cdot x$ is specialized further on below. The momenta $p, p_{1,2,3}$ and k are four-vectors as well, and γ^μ stands for Dirac’s gamma matrices. Transforming the

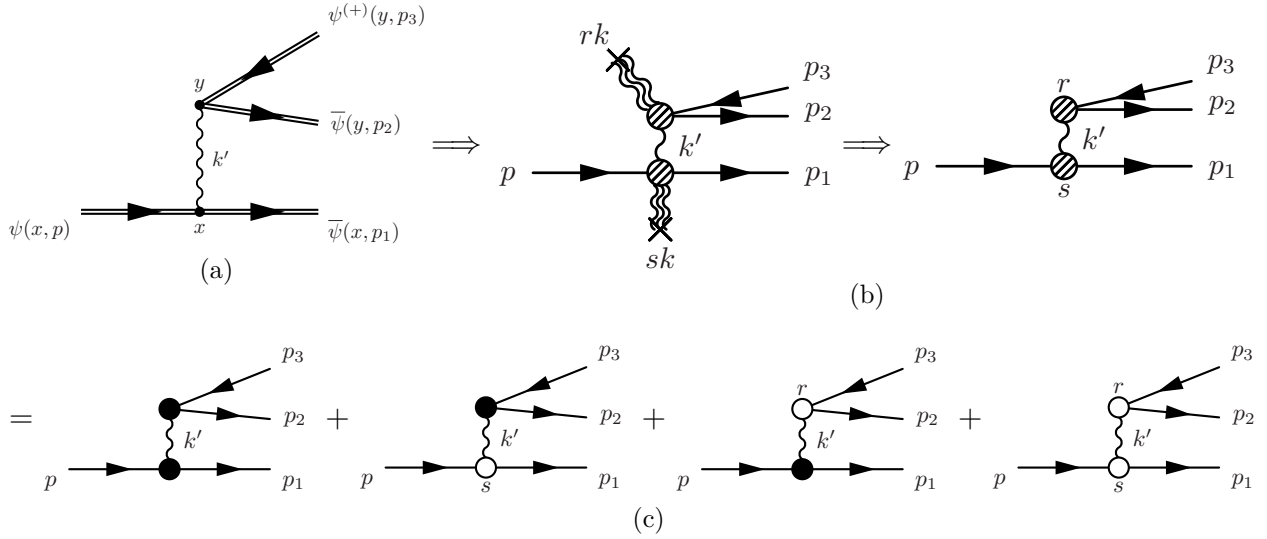


Figure 1. Diagrams for the trident process. (a) Lowest order Feynman diagram in position space Furry picture with $\Rightarrow = \psi(x, p)$ for the Volkov state, $\bullet = -ie \int d^4x \gamma^\mu$ for the vertex at x , $\sim = D_{\mu\nu}(x - y)$ for the bare photon propagator. (b) The translation into momentum space to arrive at the right diagram with \Rightarrow for the free Dirac spinor, $\otimes_s = -ie \int \frac{ds}{2\pi} \Gamma^\mu(s, p, p_1)$ with local four-momentum balance, e.g. $p + sk = k' + p_1$ and $\sim = D_{\mu\nu}(k') = \frac{ig_{\mu\nu}}{k'^2 + i\epsilon}$ for the bare photon propagator in Feynman gauge. (c) Using the regularized vertex $\bigcirc_s = -ie \int \frac{ds}{2\pi} \Gamma_{\text{reg}}^\mu(s, p, p_1)$ from $\Gamma_0^\mu = \mathcal{G}\pi\delta(s) + \Gamma_{00}^\mu$ in $\Gamma^\mu = \Gamma_0^\mu + \Gamma_1^\mu + \Gamma_2^\mu$, i.e. $\Gamma_{\text{reg}}^\mu = \Gamma_{00}^\mu + \Gamma_1^\mu + \Gamma_2^\mu$ and the one photon vertex $\bullet = \mathcal{G}\pi\delta(s)\gamma^\mu$. We note $\Gamma_1^\mu \propto ea_0$, $\Gamma_2^\mu \propto (ea_0)^2$, while Γ_{00}^μ has terms $\propto ea_0$ and $\propto (ea_0)^2$.

photon propagator into momentum space, $D_{\mu\nu}(x, y) = \int d^4k' / (2\pi)^4 e^{-ik' \cdot (x-y)} D_{\mu\nu}(k')$ and employing the Feynman gauge, $D_{\mu\nu}(k') = \frac{g_{\mu\nu}}{k'^2 + i\epsilon}$, and a suitable splitting of phase factors of the Volkov solution, e.g. $\psi(x; p) = \left(1 + e^{\frac{k \cdot A}{2p \cdot k}}\right) u_p e^{-i\hat{S}_p(k \cdot x)} e^{-ip \cdot x}$, one can cast the above matrix element in the form

$$S_{fi} = (2\pi)^2 e^2 \int dr \int ds \left[(\bar{u}(p_1) \Gamma^\mu(r; C) u(p)) \frac{g_{\mu\nu}}{k'^2 + i\epsilon} (\bar{u}(p_2) \Gamma^\mu(s; BW) v(p_3)) \right. \\ \left. \times \delta^{(4)}(p_1 + p_2 + p_3 - p - (r + s)k) - (p_1 \leftrightarrow p_2) \right] \quad (2)$$

upon Fourier transform of the vertex function $(1 + \bar{\Omega}_{q_2}(k \cdot x)) \gamma^\mu (1 + \Omega_{q_1}(k \cdot x))$ $\times e^{-i(\hat{S}_{q_1}(k \cdot x) - \hat{S}_{q_2}(k \cdot x))} = \int \frac{dr}{2\pi} \Gamma^\mu(r; q_1, q_2) e^{-ir \cdot k \cdot x}$. A key for that is $\Omega_p(\phi = k \cdot x) = e^{\frac{k \cdot A}{2p \cdot k}}$ as well as $\hat{S}(\phi = k \cdot x; p) = \frac{1}{2k \cdot p} \int_0^{k \cdot x} d\phi' (2e p \cdot A(\phi') - e^2 A^2(\phi'))$ as the nonlinear Volkov phase part. The quantities $u(p)$ and $v(p)$ are a free-field Dirac bispinors, with spin indices suppressed for brevity. In intermediate steps, one meets the local energy-momentum balance $p_1 - p + k' - sk = 0$ and $p_2 + p_3 - k' - rk = 0$, which combine to the overall conservation in $\delta^{(4)}$. The corresponding representation of the matrix element in momentum space is exhibited in figure 1(b)-left, where we exposed the interaction with s and r laser photons marked by the crosses. In figure 1(b)-right, we suppress

with the currents

$$J_0^\mu(q_1, q_2) = \bar{u}(q_1) \gamma^\mu \Psi(q_2), \quad (5a)$$

$$J_1^\mu(q_1, q_2) = \frac{ma_0}{2} \bar{u}(q_1) \left[\frac{\not{\epsilon} \not{k}}{kq_1} \gamma^\mu - \gamma^\mu \frac{\not{k} \not{\epsilon}}{kq_2} \right] \Psi(q_2), \quad (5b)$$

$$J_2^\mu(q_1, q_2) = -\frac{m^2 a_0^2}{2} \frac{k^\mu}{(kq_1)(kq_2)} \bar{u}(q_1) \not{k} \Psi(q_2), \quad (5c)$$

where $\Psi(q) = u(q)$ for C and $\Psi(q) = v(q)$ for BW , respectively. The phase integrals in equation (4) read

$$B_l(s, *) = \int_{-\infty}^{\infty} d\phi f^l(\phi) \exp \left\{ i \sum_{n=0}^2 \alpha_n(s, *) \int_0^\phi d\phi' f^n(\phi') \right\}, \quad (6)$$

with

$$\alpha_0(s; q_1, q_2) = s, \quad (7a)$$

$$\alpha_1(s; q_1, q_2) = ma_0 \left(\frac{q_1 \epsilon}{kq_1} - \frac{q_2 \epsilon}{kq_2} \right), \quad (7b)$$

$$\alpha_2(s; q_1, q_2) = \frac{m^2 a_0^2}{2} \left(\frac{1}{kq_1} + \frac{1}{kq_2} \right). \quad (7c)$$

Note that in (6), l is an index (label) on the l.h.s, while it is a power on the r.h.s., as n too. An important step is the isolation of the divergent part in Γ_0^μ or B_0 . We note $\lim_{A \rightarrow 0} \Gamma^\mu(s, *) = 2\pi \delta(s) \gamma^\mu$ and regularise Γ_0^μ by inserting a damping factor $e^{-\epsilon|\phi|}$ and performing the limit $\epsilon \rightarrow 0$, similar to the method in [56], which results in $\Gamma_0^\mu(s, q_1, q_2) = \mathcal{G} \pi \delta(s) \gamma^\mu + \Gamma_0^{12}$, with $\Gamma_0^{12} = -\mathcal{P}_s \frac{1}{s} \int_{-\infty}^{\infty} d\phi \gamma^\mu e^{is\phi} e^{-i(\hat{S}_{q_1}(\phi) - \hat{S}_{q_2}(\phi))} \frac{\partial}{\partial \phi} (\hat{S}_{q_1}(\phi) - \hat{S}_{q_2}(\phi))$ or

$$B_0(s, *) = \mathcal{G} \pi \delta(s) - \mathcal{P} \left[\frac{1}{s} \sum_{j=1}^2 \alpha_j(s, *) B_j(s, *) \right], \quad (8)$$

$$\mathcal{G} = \exp \left(\sum_{i=1}^2 \alpha_i \int_0^{+\infty} f^i(\phi) d\phi \right) + \exp \left(\sum_{i=1}^2 \alpha_i \int_0^{-\infty} f^i(\phi) d\phi \right) \quad (9)$$

where \mathcal{P} means the principal value in the variable s . One can exploit in reading (4) the crossing symmetry $\Delta^\mu(r, BW = (p_2, p_3)) = \Delta^\mu(r \rightarrow s, BW \rightarrow C = (p_1, -p))$. Employing (8) with the short-hand notation $\tilde{B}_0 = -\mathcal{P} \left[\frac{1}{s} \sum_{j=1}^2 \alpha_j B_j(s, *) \right]$ and $\tilde{B}_{1,2} = B_{1,2}$ we arrive at

$$\begin{aligned} g_{\mu\nu} \Delta^\mu(r; C) \Delta^\nu(s; BW) &= \pi^2 \mathcal{G}^2 \delta(r) \delta(s) M_0 \\ &\quad + \pi \mathcal{G} \delta(r) M_{11}(s) + \pi \mathcal{G} \delta(s) M_{12}(r) \\ &\quad + M_2(r, s), \end{aligned} \quad (10)$$

where

$$M_0 = g_{\mu\nu} J_0^\mu(C) J_0^\nu(BW), \quad (11a)$$

$$M_{11}(s) = g_{\mu\nu} J_0^\mu(C) \left(\sum_{l=0}^2 \tilde{B}_l(BW) J_l^\nu(BW) \right), \quad (11b)$$

$$M_{12}(r) = g_{\mu\nu} J_0^\mu(BW) \left(\sum_{l=0}^2 \tilde{B}_l(C) J_l^\nu(C) \right), \quad (11c)$$

$$M_2(r, s) = g_{\mu\nu} \left(\sum_{l=0}^2 \tilde{B}_l(s; BW) J_l^\mu(BW) \right) \left(\sum_{l=0}^2 \tilde{B}_l(s; C) J_l^\nu(C) \right). \quad (11d)$$

These four expressions correspond to the momentum space diagrams exhibited in figure 1(c).

3 Weak-field expansion

With the argumentation given in the introduction we now attempt an expansion in powers of a_0 . We note $J_l^\mu \propto a_0^l$ and $\alpha_l \propto a_0^l$; again, l is a label (power) on the l.h.s. (r.h.s.). The leading-order terms of the phase integrals (6) thus become

$$\tilde{B}_0(s) = -\mathcal{P} \left[\frac{a_0}{s} \tilde{\alpha}_1 \int_{-\infty}^{\infty} d\phi f(\phi) e^{is\phi} \right] + \mathcal{O}(a_0^2), \quad (12a)$$

$$\tilde{B}_j(s) = \int_{-\infty}^{\infty} d\phi f^j(\phi) e^{is\phi} \left[1 + ia_0 \tilde{\alpha}_1 \int_0^\phi d\phi' f(\phi') \right] + \mathcal{O}(a_0^2), \quad (12b)$$

$$\mathcal{G} = 2 + ia_0 \tilde{\alpha}_1 \lim_{\eta \rightarrow \infty} \left(\int_0^\eta f(\phi) d\phi + \int_0^{-\eta} f(\phi) d\phi \right) + \mathcal{O}(a_0^2). \quad (12c)$$

Denoting the Fourier transform of $f(\phi)$ by

$$F(s) = \int_{-\infty}^{\infty} d\phi f(\phi) \exp\{is\phi\} \quad (13)$$

we recognize that

$$M_0 \propto a_0^0, \quad (14a)$$

$$M_{11}(s) = a_0 J_0^\mu(C) \left(-\mathcal{P} \left[\frac{\tilde{\alpha}_1(BW)}{s} F(s) \right] J_{0\mu}(BW) + \tilde{J}_{1\mu}(BW) F(s) \right) + \mathcal{O}(a_0^2), \quad (14b)$$

$$M_{12}(r) = a_0 J_0^\mu(BW) \left(-\mathcal{P} \left[\frac{\tilde{\alpha}_1(C)}{r} F(r) \right] J_{0\mu}(C) + \tilde{J}_{1\mu}(C) F(r) \right) + \mathcal{O}(a_0^2), \quad (14c)$$

$$M_2(r, s) \propto \mathcal{O}(a_0^3). \quad (14d)$$

The two delta distributions in the M_0 term in (10) enforce for the overall momentum conservation in (2) a factor $\delta^{(4)}(p_1 + p_2 + p_3 - p)$ implying a zero contribution of the M_0 term (14a). In the spirit of the a_0 series expansion we neglect (14d) at all. (This term

would give rise to on/off-shell contributions which require some care.) The remaining leading order terms in (14b) and (14c) generate the contributions

$$S_s = 4\mathcal{G}\pi^3 e^2 \int_{-\infty}^{\infty} ds \frac{M_{11}(s)}{(p-p_1)^2 + i\epsilon} \delta^{(4)}(p_1 + p_2 + p_3 - p - sk), \quad (15a)$$

$$S_r = 4\mathcal{G}\pi^3 e^2 \int_{-\infty}^{\infty} dr \frac{M_{12}(r)}{(p_2 + p_3)^2 + i\epsilon} \delta^{(4)}(p_1 + p_2 + p_3 - p - rk) \quad (15b)$$

plus the corresponding exchange terms upon $p_1 \leftrightarrow p_2$. Introducing light-front coordinates[§] and the light-front delta distribution $\delta^{\text{lf}}(p) = \delta(p^-)\delta^{(2)}(p^\perp)$ as well as choosing k^+ as the non-zero component of the laser four-momentum k^μ yields

$$S_s = \frac{2\mathcal{G}\pi^3 e^2}{k^+} \delta^{\text{lf}}(p_1 + p_2 + p_3 - p) \frac{M_{11}(s)}{(p-p_1)^2 + i\epsilon}, \quad (16a)$$

$$S_r = \frac{2\mathcal{G}\pi^3 e^2}{k^+} \delta^{\text{lf}}(p_1 + p_2 + p_3 - p) \frac{M_{12}(r)}{(p_2 + p_3)^2 + i\epsilon}, \quad (16b)$$

where M_{11} refers to (11b) and M_{12} to (11c) and one has to use in both cases

$$r = s = \frac{p^+ - p_1^+ - p_2^+ - p_3^+}{k^+} \neq 0, \quad (17)$$

and the principal value can be dropped due to the last inequality. For given entry channel parameters, equation (17) implies the dependence $s(E_{2,3}, \cos \theta_{2,3}, \varphi_{2,3})$ with spherical coordinates $E_i, \cos \theta_i, \varphi_i$ for the particles 1, 2 and 3 (cf. figure 1(a)) in the exit channel. Fixing $E_3, \cos \theta_{2,3}$ and φ_3 yields the contour plot $s(E_2, \varphi_2)$. An example is exhibited in figure 3. The locus of the apparent one- (two-) photon contribution with $s = 1$ ($= 2$) is highlighted by fat curves.

The final result is the leading-order matrix element

$$S_{fi} = \frac{2\mathcal{G}\pi^3 e^2}{k^+} a_0 \left[\frac{M(s; BW)}{(p-p_1)^2 + i\epsilon} + \frac{M(s; C)}{(p_2 + p_3)^2 + i\epsilon} \right] F(s) \delta^{\text{lf}}(p_1 + p_2 + p_3 - p) \quad (18)$$

with

$$M(s; BW) = g_{\mu\nu} J_0^\mu(C) \left(\frac{\tilde{\alpha}_1(BW)}{s} J_0^\nu(BW) + \tilde{J}_1^\nu(BW) \right), \quad (19a)$$

$$M(s; C) = g_{\mu\nu} J_0^\mu(BW) \left(\frac{\tilde{\alpha}_1(C)}{s} J_0^\nu(C) + \tilde{J}_1^\nu(C) \right), \quad (19b)$$

where the tildes indicate here that the factor a_0 is scaled out. These structures are suggestive: $M(BW)$ may be read as the coupling of the free Compton current $J_0^\mu(C)$ to the modified Breit-Wheeler current (in parenthesis of (19a)) and a free Breit-Wheeler current $J_0^\mu(BW)$ to a modified Compton current (in parenthesis of (19b)), both depicted in the middle panels of figure 1(c). The interaction with the external field is encoded in

[§] We use the definition $q^\pm = \frac{1}{2}(q^0 \pm q^3)$ and $q^\perp = (q^1, q^2)$ for the light-front coordinates of a four-vector $q^\mu = (q^0, q^1, q^2, q^3)$.

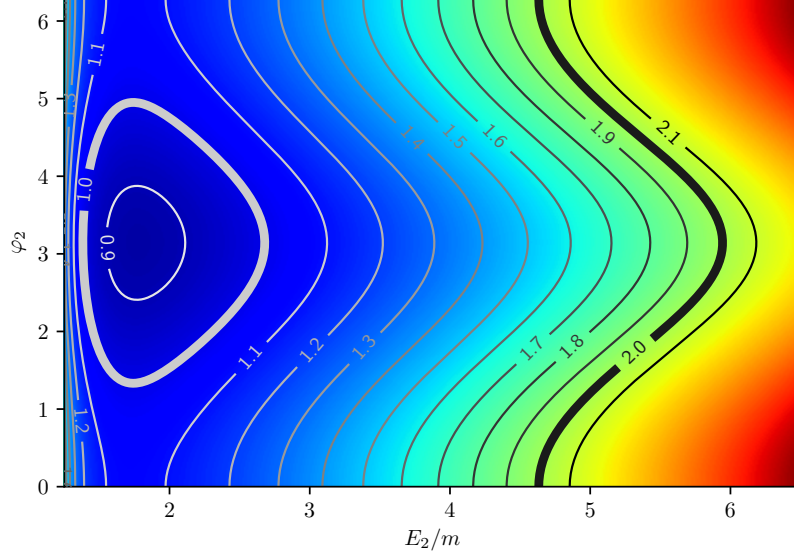


Figure 3. Contour plot $s(E_2, \phi_2)$ for $E_3 = 1.76 m$, $\cos \theta_{2,3} = 0.965$ and $\varphi_3 = 0$. The initial electron is at rest in this frame, and laser frequency amounts to $\omega = k_0 = 5.12 m$, i.e. the center of momentum energy is $\sqrt{(k+p)^2} = 3.353 m$.

the modified currents. For practical purposes we replace the modified currents by the proper Volkov currents $\Delta^\mu(C)$ and $\Delta^\mu(BW)$ when evaluating numerically the matrix elements for $a_0 \ll 1$. The differential probability is

$$dw = \left(\frac{2\mathcal{G}\pi^3 e^2}{k^+} \right)^2 |\mathcal{M}|^2 (2\pi)^3 \delta^{\text{lf}}(p_1 + p_2 + p_3 - p) |F(s)|^2 V_{\text{lf}} d\Pi_3 \quad (20)$$

with three-body phase space element

$$d\Pi_3 = \frac{\Theta(p_1^-)\Theta(p_2^-)\Theta(p_3^-)}{(2\pi)^9} \frac{dp_1^-}{2p_1^-} \frac{d^2 p_1^\perp}{2p_1^-} \frac{dp_2^-}{2p_2^-} \frac{d^2 p_2^\perp}{2p_2^-} \frac{dp_3^-}{2p_3^-} \frac{d^2 p_3^\perp}{2p_3^-}, \quad (21)$$

the Heaviside step-function Θ and the differential cross section is

$$d\sigma = \frac{dw}{NV_{\text{lf}}} \quad (22)$$

with the light-front volume V_{lf} and the normalisation factor $N = \frac{a_0^2 m^2}{2e^2} \int_{-\infty}^{\infty} g^2(\phi) d\phi$ (cf. [16]). The matrix element \mathcal{M} is given by (18) but without the pre-factor:

$$\mathcal{M} = \frac{M(s; BW)}{(p - p_1)^2 + i\epsilon} + \frac{M(s; C)}{(p_2 + p_3)^2 + i\epsilon}. \quad (23)$$

We emphasize that the weak-field limit (18) in (20) corresponds to the standard perturbative tree level QED diagrams depicted in the figure 2, supposed

$$|F(s)|^2 \rightarrow \delta(s - 1) + \delta(s + 1). \quad (24)$$

$s = 1$ selects then the admissible kinematics, and the phase space in (20) becomes five-dimensional. The decomposition (8) is essential for catching the proper weak-field perturbative limit. This is obvious when considering Møller or Bhabha scattering in an ambient background field as the cross channels of the trident process: For $A \rightarrow 0$ the standard perturbative QED must be recovered.

4 The case of a \cos^2 envelope

We now specialise the linearly polarised external e.m. field A^μ with $\varepsilon^\mu = (0, 1, 0, 0)$ to a \cos^2 envelope times the oscillating part yielding

$$f(\phi) = \left[\cos^2 \left(\frac{\pi\phi}{2\Delta\phi} \right) \cap \left(\frac{\phi}{2\Delta\phi} \right) \right] \cos(\phi + \phi_{\text{cep}}), \quad (25)$$

where $\cap \left(\frac{\phi}{2\Delta\phi} \right)$ is a box profile of width $2\Delta\phi$ centred at $\phi = 0$. We leave a discussion of the carrier envelope phase ϕ_{cep} for separate work, i.e. put $\phi_{\text{cep}} = 0$. Then (13) can be integrated analytically with the result

$$\frac{1}{\Delta\phi} F(s, \Delta\phi) = \frac{\pi^2}{2} \left[\frac{\text{sinc}(\Delta\phi(s-1))}{\pi^2 - \Delta\phi^2(s-1)} + \frac{\text{sinc}(\Delta\phi(s+1))}{\pi^2 - \Delta\phi^2(s+1)} \right], \quad (26)$$

where $\text{sinc}(x) = \frac{\sin(x)}{x}$ for $x \neq 0$ and $\text{sinc}(0) = 1$ is the cardinal sine function. With a proper normalisation, (20) is proportional to $\frac{|F(s)|^2}{\Delta\phi}$. $F(s)$ is a real function due to the even symmetry of the special field (25), but in general it acquires also an imaginary part. We therefore keep the notation $|F(s)|^2$. Given the properties of the sinc functions entering (26) we find

$$\lim_{\Delta\phi \rightarrow \infty} \frac{|F(s)|^2}{\Delta\phi} = \frac{1}{4} (\delta(s+1) + \delta(s-1)), \quad (27)$$

thus making (24) explicit. Since $\frac{|F(s)|^2}{\Delta\phi} > 0$ for $s \neq 1$, in particular for $s > 1$, at finite values of $\Delta\phi$, we see that this signals bandwidth effects, despite $a_0 \ll 1$. Such effects have been observed in [50] for the Breit-Wheeler pair production below the threshold and the Compton process as well [22, 23]. Since s is a continuous variable one must not identify it with a “photon number”; instead, s could be interpreted as fraction of energy or momentum in units of $\omega = |\vec{k}|$ participating in creating a final state different from the initial state (see [9] for discussions of that issue). Even more, $s > 1$ does not mean proper multiphoton effects due to our restriction on leading order in a_0 , rather one could speak an “apparent multiphoton effects” caused by finite bandwidth of the pulse. The dependence of $\frac{|F(s)|^2}{\Delta\phi}$ on s for various values of $\Delta\phi$ is displayed in figure 4. The function is symmetric, $|F(s)|^2 = |F(-s)|^2$, with main maxima at $s = \pm 1$ and the envelopes are

$$\frac{|F(s)|^2}{\Delta\phi} = \frac{1}{\Delta\phi} \left| \int_{-\infty}^{\infty} d\phi 2\Theta(\phi) f(\phi) e^{is\phi} \right|^2. \quad (28)$$

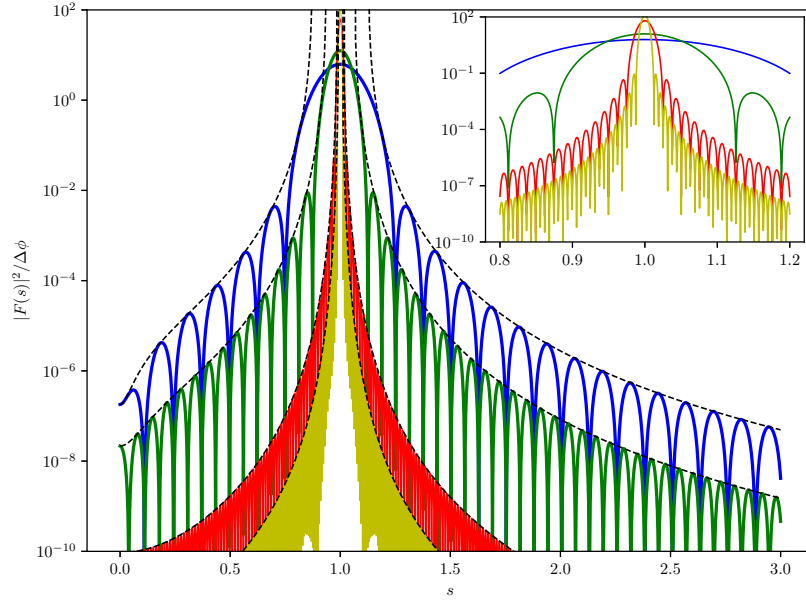


Figure 4. The quantity $\frac{|F(s)|^2}{\Delta\phi}$ as a function of s for several values of $\Delta\phi$ (blue: $\Delta\phi = 25$, green: $\Delta\phi = 50$, red: $\Delta\phi = 250$, yellow: $\Delta\phi = 500$). Dashed curves exhibit the envelopes according to equation (26). The inset zooms into the region $s \approx 1$. Note the symmetry property $|F(s)|^2 = |F(-s)|^2$.

We use the absolute value of the analytic signal of $F(s)$, i.e. the Fourier transform of the amplitude function (25) constrained to the positive half-line [57]. The first side maxima are located between $1 \pm 2\frac{\pi}{\Delta\phi}$ and $1 \pm 3\frac{\pi}{\Delta\phi}$ and their heights are 7×10^{-4} of the respective main maximum, meaning that their contribution is not negligible, in particular for a kinematical situation where $s > 1$ (cf. figure 3)

From the definition of s in equation (17), we note (i) the dependence $s(E_2, E_3, \theta_{2,3}, \varphi_{2,3})$ and (ii) the U shape of $s(E_2)$ when keeping constant the other variables of the momenta in polar coordinates. Denoting the minimum of $s(E_2)$ by s_{\min} , then for kinematical situations, where $s_{\min} > 1$ the side peaks of $\frac{|F(s)|^2}{\Delta\phi}$ with spacing of about $\frac{\pi}{\Delta\phi}$ become relevant. In fact, $\frac{|F(s)|^2}{\Delta\phi}$ carries much of the energy dependence of the differential cross section. As an example, we exhibit in figure 5 (bottom) the differential cross section $d^6\sigma / (dE_2 d\cos\theta_2 d\varphi_2 dE_3 d\cos\theta_3 d\varphi_3)$ (multiplied by m^4 to make it dimensionless) as a function of E_2 and compare it with $\frac{|F(s(E_2), \Delta\phi)|^2}{\Delta\phi}$ scaled by a factor 5.2×10^{-7} . Note the near-perfect match.|| The selected kinematics implies $s_{\min} \approx 1.1$, i.e. in the limit $\Delta\phi \rightarrow \infty$, this setting would be kinematically forbidden, but bandwidth effects for finite values of $\Delta\phi$ enable the selected kinematics. In fact, increasing $\Delta\phi$ causes (i) a rapid dropping of the differential cross section and (ii) make the oscillatory pattern more dense. At the heart of the behavior is essentially the quantity $\frac{|F(s, \Delta\phi)|^2}{\Delta\phi}$ of figure 4; the

|| Supposed the match of the cross section (22) and $\frac{|F(s, \Delta\phi)|^2}{\Delta\phi}$ scaled by one common factor continues over a wide region in phase space one could envisage a greatly simplified numerical procedure by evaluation (or even estimating) (22) only a few times and continue it with $\frac{|F(s, \Delta\phi)|^2}{\Delta\phi}$.

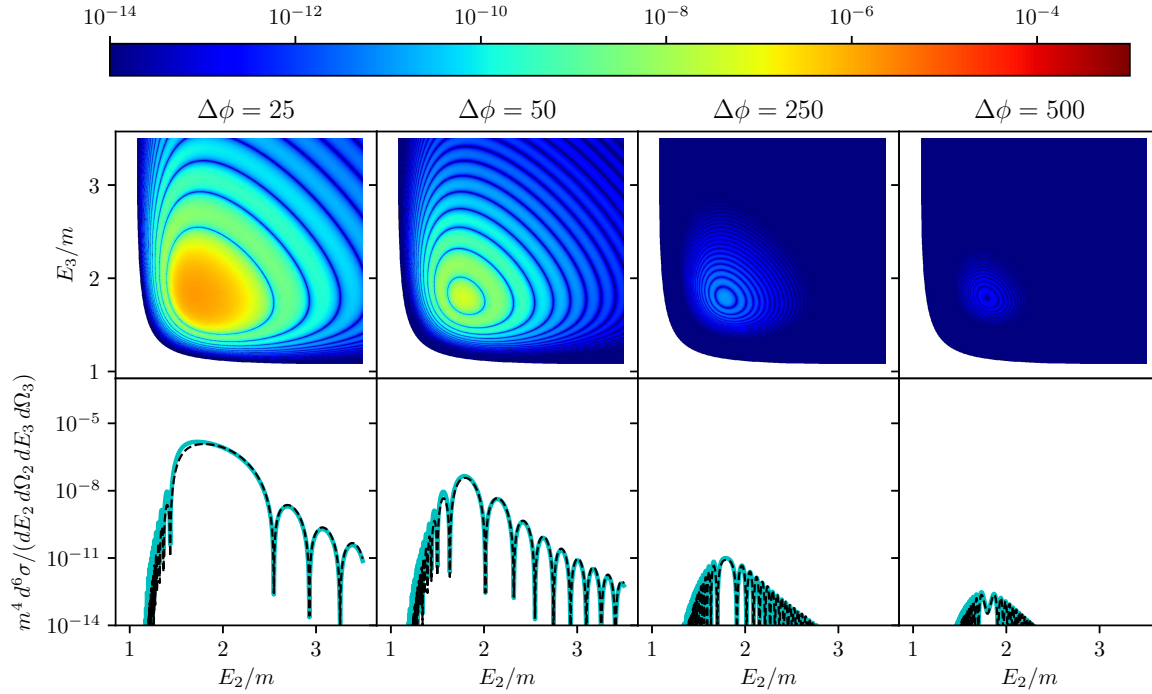


Figure 5. The differential cross section $d^6\sigma / (dE_2 d^2\Omega_2 dE_3 d^2\Omega_3)$ from equation (22) with (19a) and (19b) for an intensity parameter $a_0 = 10^{-4}$ with $d^2\Omega_{2,3} = d \cos \theta_{2,3} d\varphi_{2,3}$ for $\cos \theta_{2,3} = 0.95$, $\varphi_2 = \pi/2$, $\varphi_3 = 0$ over the $E_2 - E_3$ plane (top) and as a function of E_2 for $E_3 = 1.76m$ (bottom, solid cyan curves). The initial electron is at rest and the laser frequency amounts to $\omega = k^0 = 5.12m$ in this frame. The pulse length parameters are $\Delta\phi = 25, \dots, 500$ as indicated. In the bottom panels, the function $|F(s, \Delta\phi)|^2 / \Delta\phi$ is exhibited by dashed black curves, scaled up by a common factor of 5.2×10^{-7} .

additional E_2 dependence is fairly smooth. To translate $\frac{|F(s, \Delta\phi)|^2}{\Delta\phi}$ of figure 4 into the bottom panels of figure 5 one needs explicitly $s(E_2)$ which can be inferred from figure 3.

Displaying the differential cross section as contour plot over the $E_2 - E_3$ plane (see figure 5-top) and keeping $\theta_{2,3}$ and $\varphi_{2,3}$ fixed as above, one observes a pronounced fringe pattern which become denser with increasing values of $\Delta\phi$. The fringe pattern occupies a finite region in the $E_2 - E_3$ plane. At the origin of the fringe pattern is again the function $\frac{|F(s(E_2), \Delta\phi)|^2}{\Delta\phi}$. The fringe pattern make numerical integrations towards total cross section fairly challenging.

The relevance of the function $\frac{|F|^2}{\Delta\phi}$ continues of course for kinematical situations which are not forbidden in the limit $\Delta\phi \rightarrow \infty$. Examples are exhibited in figure 6. For the selected kinematic situation, $s_{min} = 0.976$, meaning that with increasing values of $\Delta\phi$ the differential cross section does not drop but gets concentrated at two values of E_2 (at given E_3) which are allowed for $s = 1$. In the limit $\Delta\phi \rightarrow \infty$, two delta peaks arise when E_3 is appropriately fixed. They are the result of cutting the strength distribution over the $E_2 - E_3$ plane at $E_3 = \text{const.}$, i.e. there is a sharp ring given by the solution of

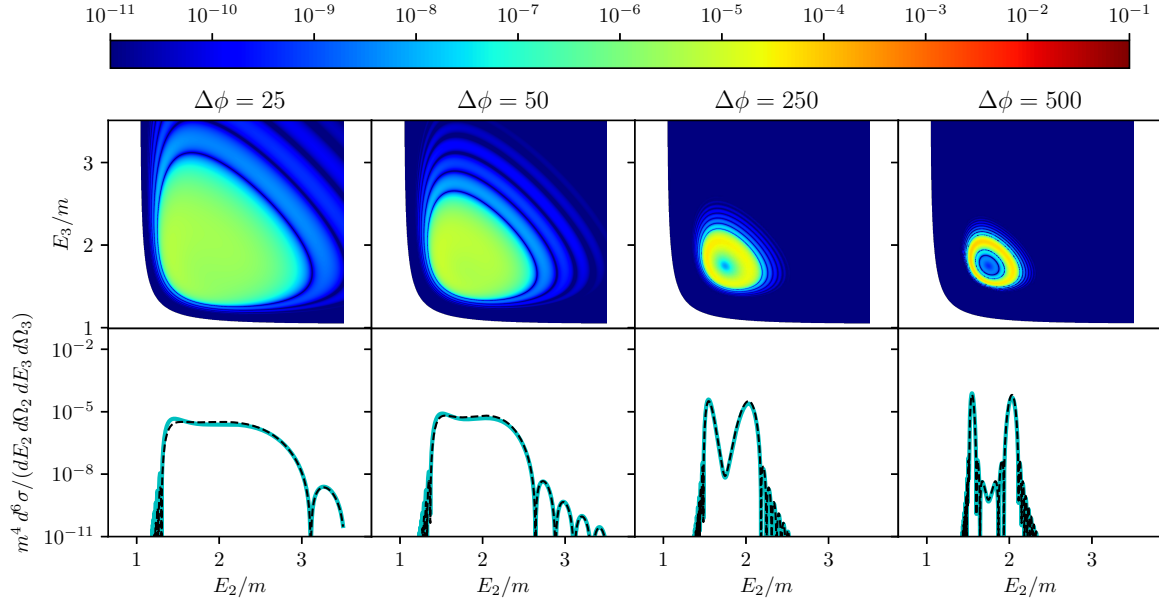


Figure 6. As figure 5 but for $\cos\theta_{2,3} = 0.965$ and the same scaling factor of $\frac{|F(s, \Delta\phi)|^2}{\Delta\phi}$. Again a near perfect agreement of the solid and dashed curves is achieved.

$E_3(E_2)$. The tilt of the U shaped function $s(E_2)$ at fixed other parameters to the right makes the region $s \approx 1$ larger at large but finite values of $\Delta\phi$. Correspondingly, the r.h.s peak structure is wider, as seen e.g. in the right bottom panel.

To compare with the standard perturbative QED (pQED) result, based on the evaluation of the Feynman diagrams depicted in figure 2, one has to perform the φ_2 integration. In fact, making $\Delta\phi$ larger and larger, the differential cross section $d^5\sigma / (dE_2 d\cos\theta_2 dE_3 d^2\Omega_3)$ from equation (22) approaches the pQED result which is for a monochromatic photon beam, see figure 7. This figure illustrates how the pQED is approached for $a_0 \ll 1$ and $\Delta\phi \rightarrow \infty$. It also demonstrates that for $\Delta\phi < 100$ a significantly larger phase space beyond the perturbatively accessible (one-photon) region (indicated by \longleftrightarrow) is occupied due to bandwidth effects in laser pulses.

5 Summary

The length of laser pulses has a decisive impact on the pair production in the trident process. The rich phase space patterns, already found and analysed in some detail for non-linear one-vertex processes à la Compton and Breit-Wheeler, show up also in the two-vertex trident process. Even for weak laser fields, a region becomes accessible which would be kinematically forbidden in a strict perturbative, leading-order tree level QED approach. The key is the frequency distribution in a pulse which differs significantly from a monochromatic laser beam, which would mean an “infinitely long laser pulse”. By resorting to a special pulse model $\propto \cos^2(\pi\phi/2\Delta\phi) \cos(\phi)$, we quantify in a transparent manner the effect of the pulse duration $\Delta\phi$ and identify the transition to monochromatic

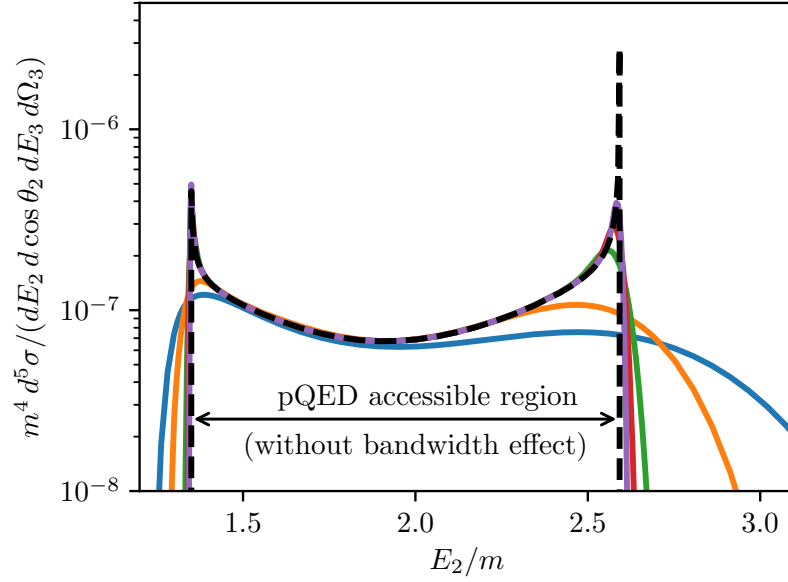


Figure 7. The differential cross section $d^5\sigma / (dE_2 d \cos \theta_2 dE_3 d^2\Omega_3)$ from (22) with (19a) and (19b) as a function of E_2/m for $E_3 = 2.0m$, $\cos \theta_{2,3} = 0.965$ and $\varphi_3 = 0$ for various values of $\Delta\phi$ (solid curves, $\Delta\phi = 25$: blue, 50: orange, 250: green, 500: red) at $a_0 = 10^{-4}$. The initial electron is at rest and the laser frequency amounts to $\omega = k^0 = 5.12m$ in this frame. The pQED result is depicted by the black dashed curve (we checked our pQED-software package by comparing with [58, 59, 60] and get confidence of our numerical evaluation and normalisation of (22) by the smooth approach towards the pQED result for large values of $\Delta\phi$).

laser fields, $\Delta\phi \rightarrow \infty$, for small values of the classical laser non-linearity parameter. To ensure the contact to a perturbative QED approach the proper decomposition of a phase factor is mandatory. To be specific, the first term in (8) is essential for the two-vertex process; for one-vertex processes it does not contribute. The effect of short laser pulses manifests itself in bandwidth effects mimicking apparent multiphoton contributions even for weak fields, where the intermediate photon is off-shell and the process is of one-step nature. The rich pattern of the differential phase space distribution is traced back to the Fourier transform of the external e.m. field. In obvious further extensions of our approach, more general pulse envelope shapes should be studied, e.g. within the slowly varying envelope approximation. Going to larger values of the classical laser non-linearity parameter means checking whether an analog of the Fourier transform of the e.m. field can be isolated as crucial element of the phase space distribution of produced particles[¶]. The final state phase distribution is important for planing corresponding experimental designs.

[¶] In fact, for $a_0 < 0.01$ and large values of $\Delta\phi$ we find numerical agreement of (22) and the pQED result.

Acknowledgments

The authors gratefully acknowledge the collaboration with A. Otto and very useful discussions with F. Mackenroth. We appreciate conversations with our colleges B. King, A. M. Fedotov, G. Torgrimsson, A. Di Piazza, A. Ilderton, T. Heinzl, A. Hartin, A. I. Titov, D. Seipt, M. Bussmann and T. Nousch. The work is supported by R. Sauerbrey and T. E. Cowan w.r.t. the study of fundamental QED processes for HIBEF.

References

- [1] G. A. Mourou, T. Tajima, and S. V. Bulanov. Optics in the relativistic regime. *Rev. Mod. Phys.*, 78:309–371, 2006.
- [2] V. Yanovsky, V. Chvykov, G. Kalinchenko, P. Rousseau, T. Planchon, T. Matsuoka, A. Maksimchuk, J. Nees, G. Cheriaux, G. Mourou, and K. Krushelnick. Ultra-high intensity-300-TW laser at 0.1 Hz repetition rate. *Opt. Express*, 16(3):2109–2114, 2008.
- [3] A. Di Piazza, C. Müller, K. Z. Hatsagortsyan, and C. H. Keitel. Extremely high-intensity laser interactions with fundamental quantum systems. *Rev. Mod. Phys.*, 84:1177, 2012.
- [4] G. A. Mourou, G. Korn, W. Sandner, and J. L. Collier, editors. *ELI White Book*. THOSS Media GmbH, 2011.
- [5] D. N. Papadopoulos, J. P. Zou, C. Le Blanc, G. Cheriaux, P. Georges, F. Druon, G. Mennerat, P. Ramirez, L. Martin, A. Frénaux, A. Beluze, N. Lebas, P. Monot, F. Mathieu, and P. Audebert. The Apollon 10 PW laser: Experimental and theoretical investigation of the temporal characteristics. *High Power Laser Sci.*, 4, 09 2016.
- [6] L. Yu, Y. Xu, Y. Liu, Y. Li, S. Li, Z. Liu, W. Li, F. Wu, X. Yang, Y. Yang, et al. High-contrast front end based on cascaded XPWG and femtosecond OPA for 10-PW-level Ti: sapphire laser. *Optics express*, 26(3):2625–2633, 2018.
- [7] A. Ringwald. Pair production from vacuum at the focus of an X-ray free electron laser. *Phys. Lett.*, B510:107–116, 2001.
- [8] A. I. Nikishov and V. I. Ritus. Quantum Processes in the Field of a Plane Electromagnetic Wave and in a Constant Field 1. *Sov. Phys. JETP*, 19:529–541, 1964. [*Zh. Eksp. Teor. Fiz.* 46:776(1964)].
- [9] V. I. Ritus. Quantum effects of the interaction of elementary particles with an intense electromagnetic field. *J. Sov. Laser Res.*, 6(5):497–617, 1985.
- [10] F. Mackenroth and A. Di Piazza. Nonlinear Compton scattering in ultra-short laser pulses. *Phys. Rev.*, A83:032106, 2011.
- [11] K. Krajewska, M. Twardy, and J. Z. Kamiński. Supercontinuum and ultrashort-pulse generation from nonlinear Thomson and Compton scattering. *Phys. Rev.*, A89(3):032125, 2014.
- [12] D. Seipt, V. Kharin, S. Rykovanov, A. Surzhykov, and S. Fritzsche. Analytical results for nonlinear Compton scattering in short intense laser pulses. *J. Plasma Phys.*, 82(2):655820203, 2016.
- [13] A. I. Titov, B. Kämpfer, A. Hosaka, T. Nousch, and D. Seipt. Determination of the carrier envelope phase for short, circularly polarized laser pulses. *Phys. Rev.*, D93(4):045010, 2016.
- [14] D. Seipt and B. Kämpfer. Laser assisted Compton scattering of X-ray photons. *Phys. Rev.*, A89(2):023433, 2014.
- [15] D. Seipt and B. Kämpfer. Asymmetries of azimuthal photon distributions in non-linear Compton scattering in ultra-short intense laser pulses. *Phys. Rev.*, A88:012127, 2013.
- [16] D. Seipt and B. Kämpfer. Non-Linear Compton Scattering of Ultrashort and Ultraintense Laser Pulses. *Phys. Rev.*, A83:022101, 2011.
- [17] T. Heinzl, D. Seipt, and B. Kämpfer. Beam-Shape Effects in Nonlinear Compton and Thomson Scattering. *Phys. Rev.*, A81:022125, 2010.

- [18] N. B. Narozhnyi and A. I. Nikishov. Pair production by a periodic electric field. *Sov. Phys. JETP*, 38:427, 1974. [*Zh. Eksp. Teor. Fiz.* 65:862(1974)].
- [19] H. R. Reiss. Absorption of light by light. *J. of Math. Phys.*, 3(1):59–67, 1962.
- [20] H. R. Reiss. Production of electron pairs from a zero-mass state. *Phys. Rev. Lett.*, 26:1072–1075, 1971.
- [21] A. I. Titov, B. Kämpfer, A. Hosaka, and H. Takabe. Quantum processes in short and intensive electromagnetic fields. *Phys. Part. Nucl.*, 47(3):456–487, 2016.
- [22] A. I. Titov, B. Kämpfer, H. Takabe, and A. Hosaka. Breit-Wheeler process in very short electromagnetic pulses. *Phys. Rev. A*, 87:042106, 2013.
- [23] A. I. Titov, H. Takabe, B. Kämpfer, and A. Hosaka. Enhanced subthreshold electron-positron production in short laser pulses. *Phys. Rev. Lett.*, 108:240406, 2012.
- [24] T. Heinzl, A. Ilderton, and M. Marklund. Finite size effects in stimulated laser pair production. *Phys. Lett.*, B692:250–256, 2010.
- [25] K. Krajewska and J. Z. Kamiński. Breit-Wheeler Process in Intense Short Laser Pulses. *Phys. Rev.*, A86:052104, 2012.
- [26] J. Z. Kamiński, M. Twardy, and K. Krajewska. Diffraction at a time grating in electron-positron pair creation from the vacuum. *Phys. Rev.*, D98(5):056009, 2018.
- [27] M. J. A. Jansen, J. Z. Kamiński, K. Krajewska, and C. Müller. Strong-field Breit-Wheeler pair production in short laser pulses: Relevance of spin effects. *Phys. Rev.*, D94:013010, 2016.
- [28] M. J. A. Jansen and C. Müller. Strong-Field Breit-Wheeler Pair Production in Two Consecutive Laser Pulses with Variable Time Delay. *Phys. Lett.*, B766:71–76, 2017.
- [29] M. J. A. Jansen and C. Müller. Strong-Field Breit-Wheeler Pair Production in Short Laser Pulses: Identifying Multiphoton Interference and Carrier-Envelope-Phase Effects. *Phys. Rev.*, D93(5):053011, 2016.
- [30] C. Bamber, S. J. Boege, T. Koffas, T. Kotseroglou, A. C. Melissinos, D. D. Meyerhofer, D. A. Reis, W. Ragg, C. Bula, K. T. McDonald, E. J. Prebys, D. L. Burke, R. C. Field, G. Horton-Smith, J. E. Spencer, D. Walz, S. C. Berridge, W. M. Bugg, K. Shmakov, and A. W. Weidemann. Studies of nonlinear QED in collisions of 46.6 GeV electrons with intense laser pulses. *Phys. Rev. D*, 60:092004, 1999.
- [31] D. L. Burke, R. C. Field, G. Horton-Smith, J. E. Spencer, D. Walz, S. C. Berridge, W. M. Bugg, K. Shmakov, A. W. Weidemann, C. Bula, K. T. McDonald, E. J. Prebys, C. Bamber, S. J. Boege, T. Koffas, T. Kotseroglou, A. C. Melissinos, D. D. Meyerhofer, D. A. Reis, and W. Ragg. Positron production in multiphoton light-by-light scattering. *Phys. Rev. Lett.*, 79:1626–1629, 1997.
- [32] C. Bula, K. T. McDonald, E. J. Prebys, C. Bamber, S. Boege, T. Kotseroglou, A. C. Melissinos, D. D. Meyerhofer, W. Ragg, D. L. Burke, R. C. Field, G. Horton-Smith, A. C. Odian, J. E. Spencer, D. Walz, S. C. Berridge, W. M. Bugg, K. Shmakov, and A. W. Weidemann. Observation of Nonlinear Effects in Compton Scattering. *Phys. Rev. Lett.*, 76:3116–3119, 1996.
- [33] H. Hu, C. Müller, and C. H. Keitel. Complete QED theory of multiphoton trident pair production in strong laser fields. *Phys. Rev. Lett.*, 105:080401, 2010.
- [34] A. Ilderton. Trident pair production in strong laser pulses. *Phys. Rev. Lett.*, 106:020404, 2011.
- [35] V. Dinu and G. Torgrimsson. Trident pair production in plane waves: Coherence, exchange, and spacetime inhomogeneity. *Phys. Rev.*, D97(3):036021, 2018.
- [36] B. King and A. M. Fedotov. Effect of interference on the trident process in a constant crossed field. *Phys. Rev.*, D98(1):016005, 2018.
- [37] F. Mackenroth and A. Di Piazza. Nonlinear trident pair production in an arbitrary plane wave: A focus on the properties of the transition amplitude. *Phys. Rev. D*, 98:116002, 2018.
- [38] T. G. Blackburn, A. Ilderton, C. D. Murphy, and M. Marklund. Scaling laws for positron production in laser–electron-beam collisions. *Phys. Rev. A*, 96:022128, 2017.
- [39] M. Altarelli, R. Brinkmann, M. Chergui, W. Decking, B. Dobson, S. Düsterer, G. Grübel, W. Graeff, H. Graafsma, J. Hajdu, J. Marangos, J. Pflüger, H. Redlin, D. Riley, I. Robinson,

- J. Rossbach, A. Schwarz, K. Tiedtke, T. Tschentscher, I. Vartanians, H. Wabnitz, H. Weise, R. Wichmann, K. Witte, A. Wolf, M. Wulff, and M. Yurkov, editors. *The Technical Design Report of the European XFEL*. DESY XFEL Project Group, 2007.
- [40] T. G. Rizzo. Kinetic Mixing and Portal Matter Phenomenology. *arXiv:1810.07531 [hep-ph]*, 2018.
 - [41] M. Bauer, P. Foldenauer, and J. Jaeckel. Hunting All the Hidden Photons. *JHEP*, 07:094, 2018.
 - [42] A. Denig. Review of dark photon searches. *EPJ Web Conf.*, 130:01005, 2016.
 - [43] T. Beranek, H. Merkel, and M. Vanderhaeghen. Theoretical framework to analyze searches for hidden light gauge bosons in electron scattering fixed target experiments. *Phys. Rev.*, D88:015032, 2013.
 - [44] F. Curciarello. Review on Dark Photon. *EPJ Web Conf.*, 118:01008, 2016.
 - [45] P. H. Adrian et al. Search for a dark photon in electroproduced e^+e^- pairs with the Heavy Photon Search experiment at JLab. *Phys. Rev.*, D98(9):091101, 2018.
 - [46] M. Raggi. Status of the PADME experiment and review of dark photon searches. *EPJ Web Conf.*, 179:01020, 2018.
 - [47] G. I. Gakh, M. I. Konchatnij, and N. P. Merenkov. Photoproduction of triplets on free electrons and the search for the dark photon. *J. Exp. Theor. Phys.*, 127(2):279–298, Aug 2018.
 - [48] M. Wing. LUXE: introduction and experiment. Technical report, European XFEL, 2017.
 - [49] A. Hartin, A. Ringwald, and N. Tapia. Measuring the Boiling Point of the Vacuum of Quantum Electrodynamics. *Phys. Rev.*, D99(3):036008, 2019.
 - [50] T. Nousch, D. Seipt, B. Kämpfer, and A. I. Titov. Pair production in short laser pulses near threshold. *Phys. Lett.*, B715:246–250, 2012.
 - [51] E. Lötstedt and U. D. Jentschura. Nonperturbative Treatment of Double Compton Backscattering in Intense Laser Fields. *Phys. Rev. Lett.*, 103:110404, 2009.
 - [52] D. Seipt and B. Kämpfer. Two-photon Compton process in pulsed intense laser fields. *Phys. Rev.*, D85:101701, 2012.
 - [53] F. Mackenroth and A. Di Piazza. Nonlinear Double Compton Scattering in the Ultrarelativistic Quantum Regime. *Phys. Rev. Lett.*, 110(7):070402, 2013.
 - [54] H. Mitter. Quantum Electrodynamics in Laser Fields. *Acta Phys. Austriaca Suppl.*, 14:397–498, 1975.
 - [55] S. Meuren, C. H. Keitel, and A. Di Piazza. Polarization operator for plane-wave background fields. *Phys. Rev.*, D88(1):013007, 2013.
 - [56] M. Boca and V. Florescu. Nonlinear Compton scattering with a laser pulse. *Phys. Rev. A*, 80:053403, 2009.
 - [57] L. Cohen. *Time-frequency Analysis: Theory and Applications*, volume 778. Prentice Hall Signal Processing Series, 1995.
 - [58] E. Haug. Bremsstrahlung and Pair Production in the Field of Free Electrons. *Z. Naturforsch.*, A30:1099–1113, 1975.
 - [59] S. Jarp and K. J. Mork. Differential cross sections for pair production by photons on electrons. *Phys. Rev. D*, 8:159–168, 1973.
 - [60] K. J. Mork. Pair production by photons on electrons. *Phys. Rev.*, 160:1065–1071, 1967.